Doppler-Only Target Motion Analysis in a High Duty Cycle Sonar System

Claude Jauffret, Annie-Claude Perez, Pierre Blanc-Benon, Hervé Tanguy

Doppler-Only Target Motion Analysis in a High Duty Cycle Sonar System

Claude Jauffret, Annie-Claude Pérez
Université de Toulon
IM2NP, UMR 7334
CS 60584
83041 TOULON Cedex 9, France
jauffret, annie-claude.perez@univ-tln.fr

Pierre Blanc-Benon, Hervé Tanguy
Airborne Acoustic Systems
THALES Underwater Systems
Route de Sainte Anne de Portzic, CS 43814
29238 Brest Cedex 3, France
Pierre.Blanc-Benon, Herve.Tanguy @fr.thalesgroup.com

Abstract*— This paper presents a new method, in an underwater context, of estimating the trajectory of a target assumed to be in constant velocity motion. The observer system is composed of a transmitter (emitting continuously, said also in high duty cycle mode) and a set of passive underwater acoustic sensors (e.g. receiving sonobuoys) not necessarily collocated with the transmitter. Each receiver detects the single-tone signal emitted by the transmitter after its reflection on the target. The two sets of doubly Doppler-shifted frequency measurements for each receiver make the target motion analysis (TMA) feasible, even when only one receiver is available. First, we develop the exact model of the bistatic received frequencies and then we compute the Cramér-Rao lower bound (CRLB) when the number of receivers is 1, 2, or 3, the measurements being corrupted by an additive and time-independent Gaussian noise. Finally, using some realistic scenarios, we show that the maximum likelihood estimated is actually efficient.

Keywords*— high duty cycle, bistatic sonar, multi-static sonar, Doppler-only TMA, estimation, Fisher Information Matrix, Cramér-Rao lower bound.

I. INTRODUCTION

Continuous transmission was first in use in the 1930s and 1940s for radar applications and electromagnetic (EM) barriers[1]. In 1984, Gough et al. [2] first proposed continuous transmission frequency modulated (CTFM) sonar in order to increase the signal-to-noise ratio and to provide continuous target location updates. The principle of bistatic sonar was pioneered by Henry Cox in his famous 1988 NATO ASI paper [1]. Cox poses the "fundamentals of bistatic active sonar", introduced by the first sentence of his paper, which summarizes perfectly the context: "*the bistatic situation is characterized by the triangle of source, target and receiver positions, and by their velocities*". The so-called high duty cycle (HDC) sonar, named also continuous active sonar (CAS), is a logical combination of both aspects. Since the publication of this article by H. Cox 27 years ago, numerous papers have become available in the open literature, dealing with several questions about HDC sonar: How many transmitters and receivers must be used to obtain a certain performance of target detection and target position estimation? How can the positions of drifting receivers and transmitters be estimated? How can ad hoc signal processing be realized? HDC sonar was studied in the late 1990s following radar applications, e.g. CTFM radar.

Among the numerous variations of HDC concepts, DeFerrari studied continuous m-codes in order to extend the temporal coherent integration time compared to single pulse sonar [3, 4]. Yang [5] proposed a continuous tracking for underwater surveillance from what he called Dopplergram, using continuous wave (CW) signals. Blanc-Benon et al. [6] studied CAS-TMA Cramér-Rao lower bound (CRLB) in a maritime patrol aircraft context with Doppler and bearing measurements from acoustic sonobuoys. In [10], Liang et al. focused on the signal processing aspect of multi-static continuous active sonar.

In this paper, we study the effect of the propagation delay on Doppler-only TMA in a HDC sonar system. The target has a constant velocity motion. We compare the behavior of the maximum likelihood estimator (MLE) when this delay is taken into account and when it is not. To do this, we consider one transmitter and one or several receiver(s) for various typical scenarios. In each of them, we derive the CRLB, the empirical bias and the empirical covariance matrix of the MLE via numerous Monte-Carlo simulations.

The paper is organized as follows:
In Section II, the exact model of a Doppler-shifted frequency is rigorously established and the common approximation in use with the monostatic sonar domain is derived. In Section III, the exact model and an approximated model are compared in the bistatic situation. Section IV is devoted to the Doppler-only TMA estimation in a bistatic situation. In particular, we illustrate by simulations that using the approximated model yields a biased MLE, whereas the exact MLE is efficient in practice. Section V presents an extension of the proposed method to multi-static situations.

[1] See https://en.wikipedia.org/wiki/History_of_radar

The conclusion addresses perspectives on HDC/CAS sonar and future enhancements regarding the sonobuoy drift problem and bearing contribution.

II. The Models of the Doppler Effect

Suppose that a source S is radiating continuously a signal $s_E(t)$. At time t, a receiver R detects the signal $s_R(t)$ defined by $s_R(t)=s_E(t-\tau(t))$. The delay $\tau(t)$ is the propagation time taken by the wave carrying the signal to reach the receiver. If the signal $s_E(t)$ is a single tone, that is $s_E(t)=a\sin(2\pi f_0 t+\varphi)$, the received signal is $s_R(t)=a'\sin[2\pi f_0[t-\tau(t)]+\varphi]$. It follows that the instantaneous frequency at time t is

$$f(t)=f_0\,(1-\dot{\tau}(t)). \qquad (1)$$

This is the exact expression of the Doppler-shifted received frequency. Consequently, the time derivative of $\tau(t)$ is needed. The delay is recursively defined by

$$\tau(t)=\frac{\|P_S(t-\tau(t))-P_R(t)\|}{c}, \qquad (2)$$

where c is the sound wave speed in the medium, $P_R(t)$ and $P_S(t)$ are the respective locations of R and S at time t. We define the range at this time as $r(t)=\|P_S(t)-P_R(t)\|$. When the source is motionless, we have $\tau(t)=\frac{r(t)}{c}$, and consequently, eq. (1) becomes

$$f(t)=f_0\left(1-\frac{\dot{r}(t)}{c}\right). \qquad (3)$$

When the source has a constant velocity V_S, the time delay $\tau(t)$ is proven to be (from (2))

$$\tau(t)=\frac{-V_S^T P_{RS}(t)+\sqrt{\left[V_S^T P_{RS}(t)\right]^2+\left(c^2-\|V_S\|^2\right)\|P_{RS}(t)\|^2}}{c^2-\|V_S\|^2}, \qquad (4)$$

with $P_{RS}(t)=P_S(t)-P_R(t)$. Consequently, the time derivative of $\tau(t)$ depends also on the motion of the receiver. Because we are concerned in the multi-static configuration by stationary receivers only, we will compute $\dot{\tau}(t)$ for a motionless receiver. Under this assumption, from (4) we get

$$\dot{\tau}(t)=-\frac{\|V_S\|^2}{c^2-\|V_S\|^2}+\frac{c^2 V_S^T P_{RS}(t)}{\left(c^2-\|V_S\|^2\right)\sqrt{\left(V_S^T P_{RS}(t)\right)^2+\left(c^2-\|V_S\|^2\right)\|P_{RS}(t)\|^2}}.$$

or equivalently

$$\dot{\tau}(t)=\frac{\dot{r}(t)}{c}\frac{1}{1-\left(\frac{v_S}{c}\right)^2}\frac{1}{\sqrt{1-\left(\frac{v_S}{c}\right)^2\sin^2\alpha(t)}}-\frac{\left(\frac{v_S}{c}\right)^2}{1-\left(\frac{v_S}{c}\right)^2}, \qquad (5)$$

where $\alpha(t)=\angle(V_S,P_{RS}(t))$, $v_S=\|V_S\|$, and $\dot{r}(t)=\|V_S\|\cos\alpha(t)=v_S\cos\alpha(t)$ (see [8]). As a consequence, we can propose two approximations of $\dot{\tau}(t)$:

First order approximation (from (5)):

$$\dot{\tau}(t)=\frac{\dot{r}(t)}{c}\left[1+\left(\frac{v_S}{c}\right)^2\right]\left[1+\frac{1}{2}\left(\frac{v_S}{c}\right)^2\sin^2\alpha(t)\right]-\frac{\left(\frac{v_S}{c}\right)^2}{1-\left(\frac{v_S}{c}\right)^2}. \qquad (6)$$

Second approximation ($v_S<<c$):

If we neglect $\left(\frac{v_S}{c}\right)^2$ in (6), we get the approximation

$$\dot{\tau}(t)\cong\frac{\dot{r}(t)}{c}. \qquad (7)$$

With this second approximation, we end up with the common expression of the Doppler-shifted frequency: $f(t)\cong f_0\left(1-\frac{\dot{r}(t)}{c}\right)$. In conclusion, when the source is in CV motion, and the receiver is motionless, the common expression of the Doppler-shifted frequency is the result of two successive approximations.

Note that, in this case, $\tau(t)=\frac{r(t-\tau(t))}{c}$.

III. The Doppler Effect in a Bistatic Configuration

In a bistatic configuration, a target T, an emitter (or transmitter) E, and a receiver R are assumed to lie on the same horizontal plane. The transmitter sends a signal continuously and the target plays the role of mirror: it reflects the signal emitted by the transmitter toward the receiver (see Fig. 1). Unlike a classic active system, the receiver stands apart from the transmitter. So, the receiver detects the signal $s_R(t)$ defined by $s_R(t)=\kappa_2\, s_{\text{Reflected}}(t-\tau_2(t))$, where $s_{\text{Reflected}}$ is the signal reflected by T, τ_2 is the propagation time of the target–receiver range, and κ_2 accounts for the attenuation due to propagation. The signal $s_{\text{Reflected}}$ is the signal emitted by E, propagation time between E and T old: $s_{\text{Reflected}}(u)=\kappa_1\, s_E(u-\tau_1(u))$, for any u, κ_1 accounts for the signal attenuation. In our configuration, E and R are motionless.

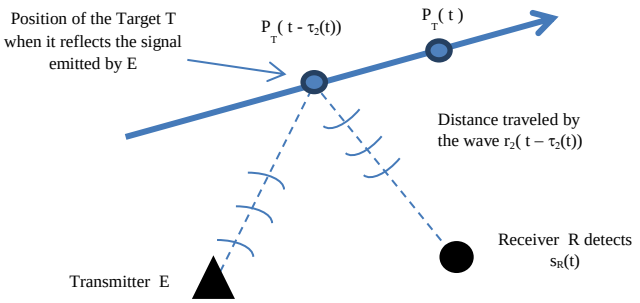

Fig. 1: Standard scenario of the bistatic HDC sonar

In the couple (E,T), the source is E; hence $\tau_1(t)=\frac{r_1(t)}{c}$. In the

couple (T, R), T plays the role of the source; therefore, $\tau_2(t)=\frac{r_2(t-\tau_2(t))}{c}$. The chain rule allows the signal detected by the receiver to be defined as $s_R(t)=\kappa_1\kappa_2\, s_E(t-\tau_2(t)-\tau_1(t-\tau_2(t)))$ for any t. Again, when s_E is a single tone with the frequency f_0, the instantaneous received frequency is

$$f(t)=f_0\left[1-\dot{\tau}_2(t)-(1-\dot{\tau}_2(t))\times\dot{\tau}_1(t-\tau_2(t))\right]. \quad (8)$$

Once more, several approximations of $f(t)$ can be proposed:

The first approximation is based upon the first-order approximation $\dot{\tau}_1(t-\tau_2(t))\cong\dot{\tau}_1(t)$. We get

$$f(t)\cong f_0\left[1-\dot{\tau}_2(t)-(1-\dot{\tau}_2(t))\dot{\tau}_1(t)\right]=f_0\left[1-\dot{\tau}_1(t)\right]\left[1-\dot{\tau}_2(t)\right]=f_1(t) \quad (9).$$

Another approximation consists of using the approximation (7) for $\dot{\tau}_2(t)$, that is $\dot{\tau}_2(t)\cong\frac{\dot{r}_2(t)}{c}$. We then get

$$f(t)\cong f_0\left[1-\frac{\dot{r}_1(t)}{c}\right]\left[1-\frac{\dot{r}_2(t)}{c}\right]=f_2(t). \quad (10)$$

A third approximation is obtained by neglecting the term $\frac{\dot{r}_1(t)\dot{r}_2(t)}{c^2}$; we end up with the common approximation used in the bistatic radar systems:

$$f(t)\cong f_0\left[1-\frac{\dot{r}_1(t)+\dot{r}_2(t)}{c}\right]=f_3(t). \quad (11)$$

An example of received frequencies versus time, for the exact model, and for the three approximated models is given hereafter. The scenario is the following: the transmitter and the receiver are respectively located at $[-3500\quad 0]^T$ (m) and $[+3500\quad 0]^T$ (m). The target has a speed of 30 m/s and a heading of 90°. At *t*=650 s, the target is at position $[0\quad 1000]^T$ (m). The transmitter emits a single tone with a frequency $f_0=1000$ Hz.

Fig. 2(a) and 2(b) depict $f(t)$ in blue, $f_1(t)$ in green, $f_2(t)$ in cyan, and $f_3(t)$ in magenta for $0\le t\le 1300$ s. We also simulated the temporal received signal $s_R(t)$, sampled at 3000 Hz, and performed an 8192-point FFT after zero-padding. The outputs of the FFT are plotted in red in Figs. 2 (a) and 2 (b), which is a magnification of Fig. 2 (a). This simulation shows that the exact model fits the frequency track produced by the spectral analysis. It also exhibits the approximation error in the three approximated models. In this example, one can see the double closest-point-of-approach (CPA) inflexion points: the first one regarding the transmitter, the second one regarding the receiver.

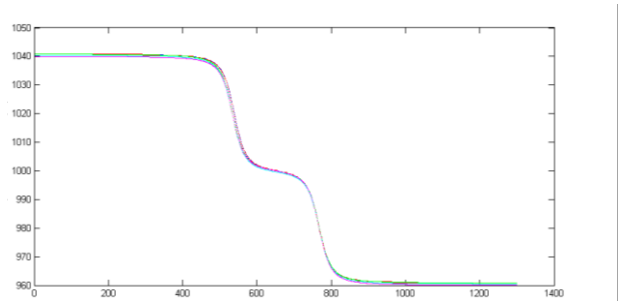

Fig. 2 (a): Frequency tracks with double inflexion CPA points (x axis: time in seconds, y axis: frequency in Hz).

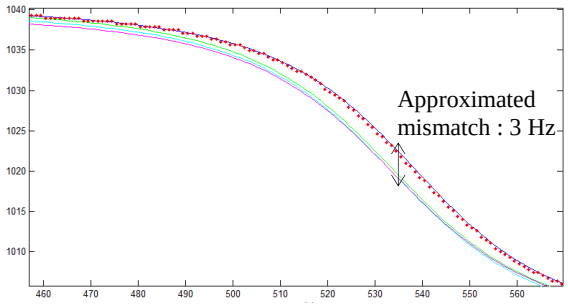

Fig. 2 (b): Magnification of the frequency tracks; the dotted line is given by the output of the FFT.

Note that in a radar bistatic system, the approximation (11) is acceptable thanks to the EM waves' speed (which is huge relative to the aircraft speed) unlike in the sonar domain.

IV. TMA IN A BISTATIC SYSTEM

A. *Problem setting*

The common configuration of a simple bistatic system consists of a transmitter E and a receiver R, both mounted on sonobuoys. In this study, they are assumed to be stationary. A target T is in CV motion and is detected only by the receiver from the signal coming from T. This signal is actually emitted by E and reflected by T toward R. The target velocity is denoted as V_T, and its position at the very beginning of the scenario is $P_T(0)$. The transmitter and the receiver are located at P_E and P_R, respectively. After an ad hoc spectral analysis, only the set of Doppler-shifted frequency measurements is available: $f_m(t_k)=f(t_k)+\varepsilon_k$, for $k=1,\cdots,K$ and ε_k the corrupting noise, which means that the sonobuoy carrying the receiver is not a directive sonobuoy [7] but rather an omnidirectional buoy. Implicitly, $f(t_k)$ is completely defined by $X=\left[P_T^T(0)\quad V_T^T\right]^T$. Our goal is to estimate X, given $f_m(t_k),\ k=1,\cdots,K$.

To do this, we have two options: (i) use the correct model given by (8); or (ii) use an approximate model. We choose to put in competition the correct model and the approximated model (11). Indeed, the correct model is expected to give better results in the estimation process, but the computational burden will definitively be heavy compared to an estimation based upon the model (11).

B. Observability

For the approximated model (11), X was proven to be observable in [11] by using the rank of the Fisher information matrix (FIM). Obviously, the state vector X is not observable since X is undistinguishable from its image by the axial symmetry around the line (ER) and from its image by the axial symmetry around the perpendicular bisector of the segment [ER]. The line [ER] and the bisector define 4 sectors of the plane. We claim that, in each sector, the condition of observability is that the target must not travel on the line defined by the couple (E, R). This will be the topic of a future paper.

For the correct model (8), observability has not been proven so far. To bypass this lack in the rest of the paper, we will consider scenarios for which the FIM is non-singular, so X is locally observable [9].

C. Fisher Information Matrix and Cramér-Rao lower bound

The classic expression of the FIM under Gaussian hypothesis is $F(X)=\sum_{k=1}^{K}\frac{1}{\sigma^2}\nabla_X f(t_k)\nabla_X^T f(t_k)$, with

$$\nabla_X f(t_k)=f_0\{[\dot\tau_2(t_k,X)-1]\nabla_X\dot\tau_1(t_k-\tau_2(t_k,X),X)+[\dot\tau_1(t_k-\tau_2(t_k,X),X)-1]\nabla_X\dot\tau_2(t_k,X)\}.$$

We have to compute the following four quantities: $\tau_1(t_k,X)$, $\tau_2(t_k,X)$, $\dot\tau_1(t_k,X)$, and $\dot\tau_2(t_k,X)$.

We end up with

$$\tau_1(t_k,X)=\frac{1}{c}\|P_1(t_k)\|=\frac{r_1(t_k,X)}{c},$$

$$\tau_2(t_k,X)=\frac{-V_T^TP_2(t_k)+\sqrt{[V_T^TP_2(t_k)]^2+(c^2-\|V_T\|^2)\|P_2(t_k)\|^2}}{c^2-\|V_T\|^2},$$

$$\dot\tau_1(t_k,X)=\frac{V_T^TP_1(t)}{c\|P_1(t)\|}=\frac{\dot r_1(t_k,X)}{c},$$

$$\dot\tau_2(t_k,X)=-\frac{\|V_T\|^2}{c^2-\|V_T\|^2}+\frac{c^2V_T^TP_2(t_k)}{(c^2-\|V_T\|^2)\sqrt{(V_T^TP_2(t_k))^2+(c^2-\|V_T\|^2)\|P_2(t_k)\|^2}}.$$

The detailed computations are presented in the Appendix.

D. Estimation

We have chosen the MLE, which is also the least squares estimator $\hat X$, that minimizes $C(X)=\sum_{k=1}^{K}\frac{1}{\sigma^2}[f_m(t_k)-f(t_k)]^2$ for the correct model (8), or the approximated MLE $\hat X_{app}$, that minimizes $C_{app}(X)=\sum_{k=1}^{K}\frac{1}{\sigma^2}[f_m(t_k)-f_3(t_k)]^2$ for the approximated model (11). Both are obtained by a numerical routine (Gauss-Newton).

E. Monte-Carlo simulations

Our analysis is based on 500 Monte-Carlo runs. In the scenarios used:

$P_E=[-3500\ \ 0]^T$ (m) and $P_R=[+3500\ \ 0]^T$ (m). The measurements are time stamped at 1 Hz rate: $t_k=(k-1)\Delta t$, with $\Delta t=1s$. The frequency f_0 is equal to 1000 Hz. We choose a reasonable standard deviation of the frequency measurement: $\sigma=0.25$ Hz. All the measurements are simulated using the correct model. The total duration is 1300s. In this configuration, we consider three targets, whose respective trajectories are defined by

$X_1=[-10{,}000\ \ -25{,}000\ \ 25\ \ 0]^T$ (the target sails eastwards),

$X_2=[-2{,}500\ \ 7{,}000\ \ 0\ \ -10]^T$ (the target sails southwards),

and $X_3=[-2{,}500\ \ 14{,}000\ \ 15\ \ -13]^T$ (the target sails towards south-east). For each target, the respective performances are presented in tables, whose first column is the empirical bias of $\hat X_{app}$, while the second column is the empirical bias of $\hat X$. The empirical standard deviations of the components of $\hat X_{app}$ and $\hat X$ are written in the third and fourth columns. The minimal standard deviations (computed from the CRLB with the correct model) of the components of X are the elements of the fifth column. Figures depict the estimate sets in the plane (x,y): the correct estimated positions are represented by blue dots, whereas the approximated estimated positions are given by red crosses. The 90% confidence ellipse is plotted in magenta.

1) Scenario 1 : $X=X_1$

TABLE I: PERFORMANCES OF $\hat X_{app}$ AND $\hat X$ AND MINIMAL STANDARD DEVIATIONS

X	Bias		$\hat\sigma$		σ_{CRLB}
	Approximated model	**Exact model**	***Approximated model***	**Exact model**	
-10000 m	*11037*	111.32	*2671.4*	2734.7	2510.5
-25000 m	*9112.7*	103.33	*2734.9*	878.85	781
25 m/s	*3.77*	0.14	*1.67*	0.23	0.15
0 m/s	*12.07*	0.07	*3.20*	2.65	2.43

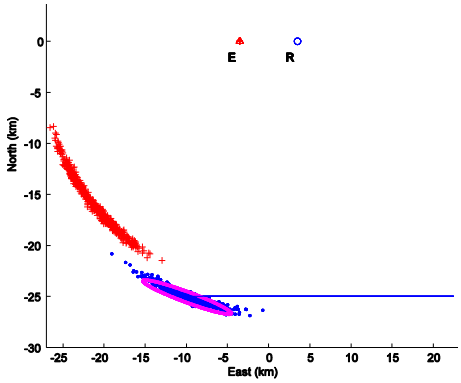

Fig. 3: Target's trajectory, initial positions estimated with exact model (blue dots) and with approximated model (red crosses), and the 90% confidence ellipse (magenta).

Note that the estimate clouds are croissant-shaped.

2) Scenario 2 : $X = X_2$

TABLE II: PERFORMANCES OF $\hat{X}_{app}$ AND $\hat{X}$ AND MINIMAL STANDARD DEVIATIONS

X	Bias		$\hat{\sigma}$		σ_{CRLB}
	Approximated model	**Exact model**	***Approximated model***	**Exact model**	
-2500 m	*61.04*	0.7	*17.17*	17.19	17 .28
7000 m	*40.37*	0.06	*5.45*	5.42	5.49
0 m/s	*0.09*	0.0015	*0.02*	0.02	0.02
-10 m/s	*0.004*	0.0003	*0.006*	0.006	0.006

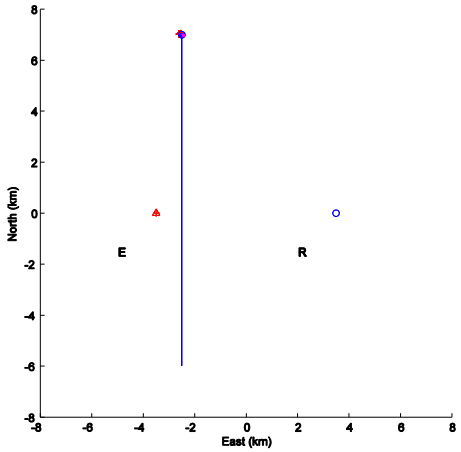

Fig. 4 (a): Target's trajectory, initial positions estimated with exact model (blue dots) and with approximated model (red crosses), and the 90% confidence ellipse (magenta).

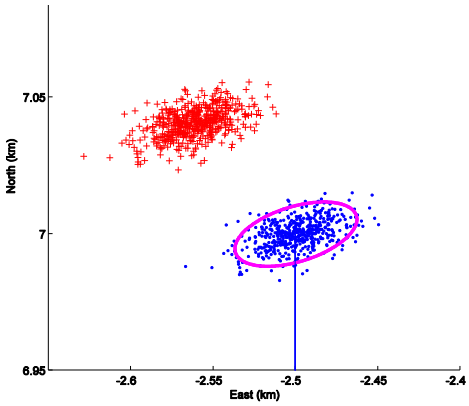

Fig. 4 (b): A magnification of the clouds of estimates of Fig. 4(a).

3) Scenario 3 : $X = X_3$

TABLE III: PERFORMANCES OF $\hat{X}_{app}$ AND $\hat{X}$ AND MINIMAL STANDARD DEVIATIONS

X	Bias		$\hat{\sigma}$		σ_{CRLB}
	Approximated model	**Exact model**	***Approximated model***	**Exact model**	
-2500 m	*4626.4*	5.97	*205.77*	255.37	254.16
14000 m	*1145.9*	4.52	*34.67*	113.9	113.04
15 m/s	*3.9*	0.003	*0.19*	0.18	0.18
-13 m/s	*4*	0.009	*0.15*	0.26	0.26

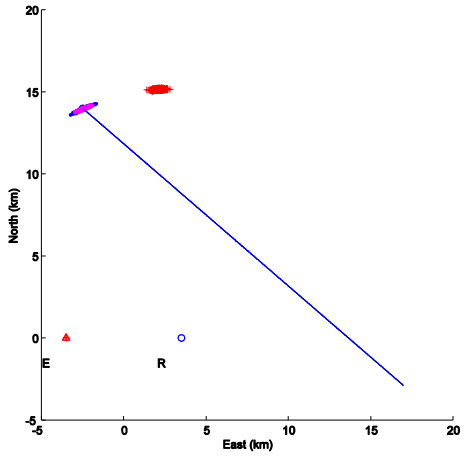

Fig. 5(a): Target's trajectory and initial positions estimated with exact model (blue dots) and with approximated model (red crosses).

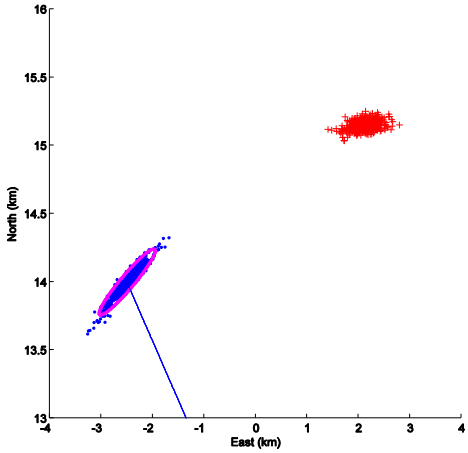

Fig. 5 (b): A magnification of the clouds of estimates of Fig. 5(a).

These simulations reveal two facts: (i) the bias induced by the approximated model is not negligible; and (ii) the MLE performs properly for the exact model (its sample covariance matrix – not reported here – is very close to the CRLB and its bias is relatively small). A legitimate question must be asked: Is this bias persistent if more than one receiver is employed? We address this question in the next section.

V. TMA IN MULTI-STATIC CONFIGURATION

When N (>1) receivers are available, we can exploit the frequency track collected by each receiver to improve the TMA. The criterion is then

$$C(X)=\sum_{n=1}^{N}\sum_{k=1}^{K_n}\frac{1}{\sigma^2}\left[f_{(n)m}(t_k)-f_{(n)}(t_k)\right]^2 \qquad (12)$$

where $f_{(n)m}(t_k)$ is the frequency measured by the receiver $\#n$ at time t_k, K_n is the number of measurements acquired by the receiver $\#n$, and $f_{(n)}(t_k)$ is the exact model. Consequently, the FIM is $F(X)=\sum_{n=1}^{N}\sum_{k=1}^{K_n}\frac{1}{\sigma^2}\nabla_X f_{(n)}(t_k)\nabla_X^T f_{(n)}(t_k)$. Note that, for the sake of simplicity in the writing of the equations, we have considered that the measurements are synchronous. But we can readily consider TMA when this is not the case: the only thing that matters is that the measurements need to be time stamped. In the following subsections, we compare the respective performances of $\hat{X}$, that minimizes (12), and of $\hat{X}_{app}$, that minimizes (12), in which we replace the correct model by the approximated model (11). This comparison is based upon scenario 1.

A. With two receivers

Since we benefit from a second set of measurements, the duration of scenario 1 is reduced to 10 min.

TABLE IV: PERFORMANCES OF $\hat{X}_{app}$ AND $\hat{X}$ AND MINIMAL STANDARD DEVIATIONS

X	Bias		$\hat{\sigma}$		σ_{CRLB}
	Approximated model	**Exact model**	***Approximated model***	**Exact model**	
-10000 m	*1619.6*	11.28	*379 .12*	452.41	449.98
-25000 m	*585.71*	3.82	*343.63*	340.82	338.88
25 m/s	*0.55*	0.001	*0.21*	0.21	0.20
0 m/s	*1.85*	0.007	*0.31*	0.37	0.37

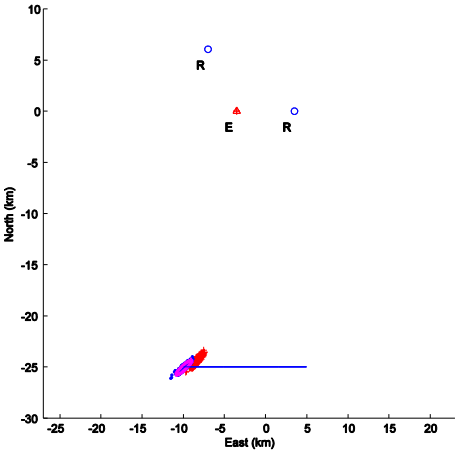

Fig. 6 (a): Target's trajectory and initial positions estimated with exact model (blue dots) and with approximated model (red crosses) in a tri-static configuration.

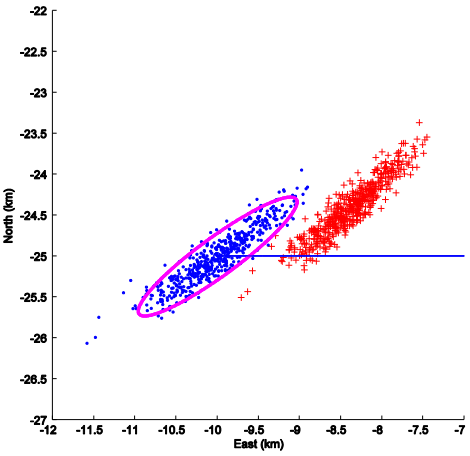

Fig. 6 (b): A magnification of the clouds of estimates of Fig. 6(a).

Fig. 6 shows that the bias is maintained when the approximated model is used. So, again we increase the number of receivers in the next subsection.

B. With three receivers

With three receivers, the duration of scenario 1 is now set to 5 min.

TABLE V: PERFORMANCES OF $\hat{X}_{app}$ AND $\hat{X}$ AND MINIMAL STANDARD DEVIATIONS

X	Bias		$\hat{\sigma}$		σ_{CRLB}
	Approximated model	**Exact model**	***Approximated model***	**Exact model**	
-10000 m	*376.69*	3.31	*59.98*	58.67	59.48
-25000 m	*186.52*	11.06	*198.56*	198.11	197.18
25 m/s	*0.06*	0.006	*0.11*	0.11	0.11
0 m/s	*0.81*	0.002	*0.07*	0.06	0.06

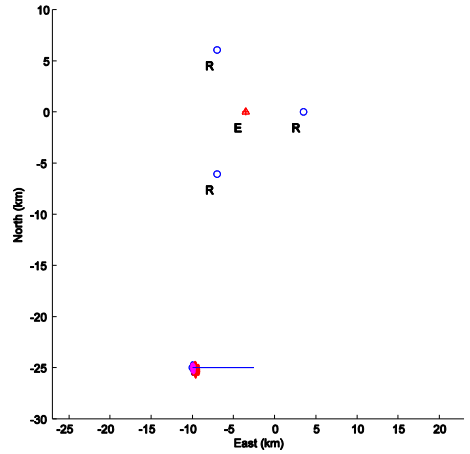

Fig. 7 (a): Target's trajectory and initial positions estimated with exact model (blue dots) and with approximated model (red crosses) in a quadri-static configuration.

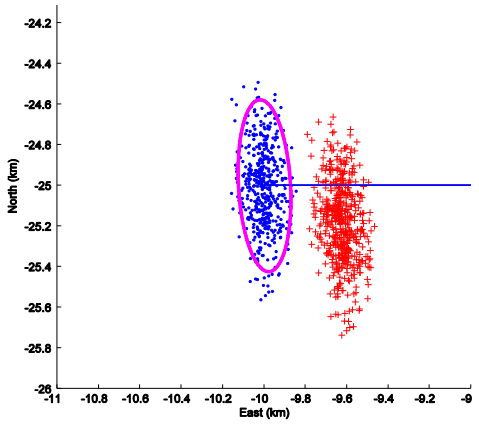

Fig. 7 (b): A magnification of the clouds of estimates of Fig. 7(a).

In Fig. 7, a non-negligible bias, whose components are given in Table V, is visible when the approximated model is used. We note a reduction of the bias with an increasing number of receivers. However, the lesson to be drawn from these simulations is clear: the approximated model provides a biased estimator. For the HDC sonar, we hence recommend to use the correct model to construct the MLE, even if it requires more computational time.

Table VI and Fig. 8 present results when simulation duration is reduced to 1 minute.

TABLE VI: PERFORMANCES OF $\hat{X}_{app}$ AND $\hat{X}$ AND MINIMAL STANDARD DEVIATIONS

X	Bias		$\hat{\sigma}$		σ_{CRLB}
	Approximated model	**Exact model**	***Approximated model***	**Exact model**	
-10000 m	*389.44*	5.72	*199.3*	230.8	230.1
-25000 m	*130.05*	14.72	*1340.4*	1337.9	1338.3
25 m/s	*0.02*	0.004	*1.02*	1.02	1.02
0 m/s	*0.78*	0.004	*0.16*	0.2	0.2

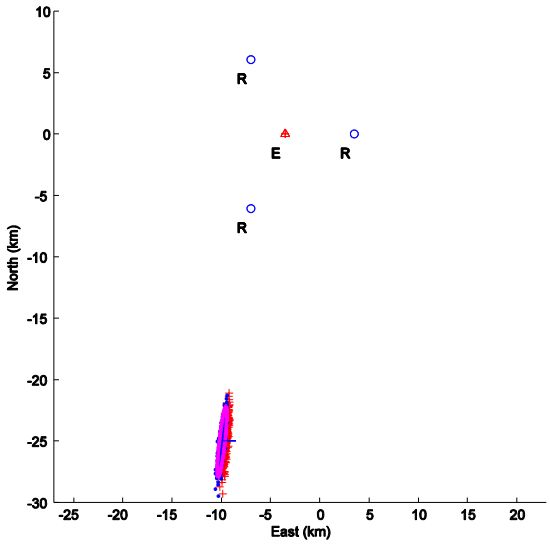

Fig. 8(a): Target's trajectory and initial positions estimated with exact model (blue dots) and with approximated model (red crosses) in quadri-static configuration.

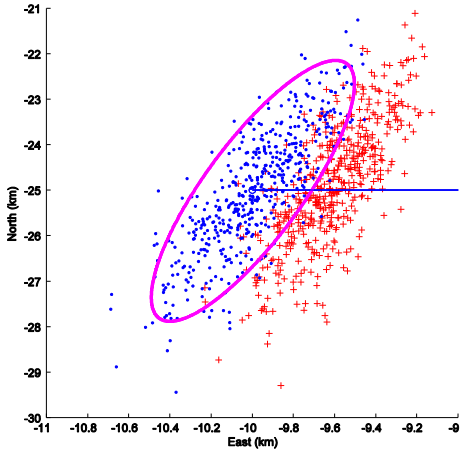

Fig. 8 (b): A magnification of the clouds of estimates of Fig. 8(a).

The good news is that the MLE estimate for an HDC sonar system has a covariance matrix compatible with an operational exploitation for short favorable scenarios (about one minute), which is an advantage in real situations where the sonobuoys carrying the transmitter and the receivers are set to drift.

VI. CONCLUSION AND PERSPECTIVES

Frequency-only TMA in a multi-static sonar configuration has been studied in this paper. Two major results were obtained: first, the approximated model, widely used in multi-static radar systems, induces a non-negligible biased estimator in sonar applications. On the contrary, the performance of MLE based upon the exact model is compatible with the asymptotic performance given by the CRLB: its empirical covariance matrix is close to the bound and it is practically unbiased. The price is an augmentation of the computation time. Finally, in short favorable scenarios, the CRLB allows us to expect TMA results that are compatible with the operational exploitation of a multi-static system (provided the number of receivers is sufficient).

As HDC sonar is becoming more and more popular [12], further studies should analyze the impact of drifting of receivers due to ocean currents and in GPS-denied areas. The contribution of bearing measurement should also be analyzed when using directive receivers in terms of duration to get a given target location accuracy compared to the case of frequency-only TMA.

APPENDIX

For convenience, hereafter we will use the notation $P_1(t) = P_{TE}(t)$, $P_2(t) = P_{RT}(t)$, and $r_i(t) = \| P_i(t) \|$, for $i = 1, 2$. We start by computing some necessary calculation elements:

$$\nabla_X \| V_T \|^2 = 2 \begin{bmatrix} 0 & 0 & V_T^T \end{bmatrix}^T ,$$

$$\nabla_X \left[\frac{\| V_T \|^2}{c^2 - \| V_T \|^2} \right] = \frac{c^2}{c^2 - \| V_T \|^2} \nabla_X \| V_T \|^2 .$$

$$\nabla_X\left[V_T^T P_i(t_k)\right]=\begin{pmatrix} V_T \\ P_i(t_k)+t_k V_T \end{pmatrix},$$

$$\nabla_X\left[V_T^T P_i(t_k)\right]^2 = 2\, V_T^T P_i(t_k)\nabla_X\left[V_T^T P_i(t_k)\right].$$

$$\nabla_X \| P_i(t_k)\|^2 = 2\begin{pmatrix} P_i(t_k) \\ t_k P_i(t_k)\end{pmatrix}.$$

$$\nabla_X\left[\, \|P_i(t_k)\|^2\left(c^2-\|V_T\|^2\right)\right] = \left(c^2-\|V_T\|^2\right)\times\nabla_X\| P_i(t_k)\|^2 . \\ -\| P_i(t_k)\|^2\times\nabla_X\|V_T\|^2$$

Let us define $a_i(t_k)=\sqrt{\left[V_T^T P_i(t_k)\right]^2+\left(c^2-\|V_T\|^2\right)\| P_i(t_k)\|^2}$.

$$\nabla_X a_i(t_k)=\frac{1}{2a_i(t_k)}\left[\nabla_X\left[V_T^T P_i(t_k)\right]^2+\left(c^2-\|V_T\|^2\right)\times\nabla_X\|P_i(t_k)\|^2\right].$$

$$\nabla_X\left[\left(c^2-\|V_T\|^2\right)a_i(t_k)\right]=\left(c^2-\|V_T\|^2\right)\nabla_X a_i(t_k)-a_i(t_k)\nabla_X\|V_T\|^2$$

$$\nabla_X\left[\frac{V_T^T P_2(t_k)}{\left(c^2-\|V_T\|^2\right)\, a_i(t_k)}\right]=\frac{\nabla_X\left[V_T^T P_2(t_k)\,\right]}{\left(c^2-\|V_T\|^2\right)\, a_i(t_k)} \\ -\frac{V_T^T P_2(t_k)}{\left(c^2-\|V_T\|^2\right)^2\, a_i^2(t_k)}\nabla_X\left[\left(c^2-\|V_T\|^2\right) a_i(t_k)\right]$$

Now, we are able to give the values of the first two gradients:

$$\nabla_X\tau_2(t_k,X)=\frac{\nabla_X\, a_2(t_k)-\nabla_X\left[V_T^T P_2(t_k)\right]}{c^2-\|V_T\|^2} \\ +\frac{a_2(t_k)-V_T^T P_2(t_k)}{\left[c^2-\|V_T\|^2\right]^2}\nabla_X\|V_T\|^2 .$$

$$\nabla_X\ \dot\tau_2(t_k)=-\nabla_X\left[\frac{\|V_T\|^2}{c^2-\|V_T\|^2}\right]+c^2\nabla_X\left[\frac{\left(V_T^T P_2(t_k)\right)}{\left(c^2-\|V_T\|^2\right) a_2(t_k)}\right].$$

Computation of $\nabla_X\dot\tau_1(t_k-\tau_2(t_k,X),X)$:

First, we write $\dot\tau_1(t_k-\tau_2(t_k,X),X)$ as the composition of the following two functions:

$$\begin{array}{ccccc} \mathbf{R}^4 & \xrightarrow{g} & \mathbf{R}^5 & \xrightarrow{h} & \mathbf{R} \\ X & \overset{g}{\mapsto} & Y=\begin{pmatrix} t_k-\tau_2(t_k,X) \\ X\end{pmatrix}=\begin{pmatrix} u \\ X\end{pmatrix} & \overset{h=\dot\tau_1}{\mapsto} & \dot\tau_1(Y)=h\circ g(X)=\dot\tau_1(t_k-\tau_2(t_k,X),X). \end{array}$$

We readily deduce that its gradient is equal to the product of two gradients, that is $\nabla_X\dot\tau_1(t_k-\tau_2(t_k,X),X)=\nabla_X\left[h\circ g(X)\right]$

$$=\nabla_X g\ .\nabla_Y h\ \Big|_{Y=\begin{pmatrix} t_k-\tau_2(t_k,X) \\ X\end{pmatrix}}$$

with $\nabla_X g=\nabla_X\begin{pmatrix} t_k-\tau_2(t_k,X) \\ X\end{pmatrix}=\begin{pmatrix}-\nabla_X\tau_2(t_k,X) & \mathbf{I}_4\end{pmatrix}$ and

$\nabla_Y h=\begin{pmatrix} \dfrac{\partial h(u,X)}{\partial u} \\ \hline \nabla_X h\end{pmatrix}$. So we get:

$$\nabla_X\dot\tau_1(t_k-\tau_2(t_k,X),X)=\begin{pmatrix}-\nabla_X\tau_2(t_k,X) & \mathbf{I}_4\end{pmatrix}\begin{pmatrix} \dfrac{\partial h(u,X)}{\partial u} \\ \nabla_X h\end{pmatrix}$$

$$=-\frac{\partial h(u,X)}{\partial u}\nabla_X\tau_2(t_k,X)+\nabla_X h(u,X)$$

for $u=t_k-\tau_2(t_k,X)$

$$\nabla_X\dot\tau_1(t_k-\tau_2(t_k,X),X)=-\frac{\partial\dot\tau_1(u,X)}{\partial u}\nabla_X\tau_2(t_k,X)+\nabla_X\dot\tau_1(u,X),$$

for $u=t_k-\tau_2(t_k,X)$.

with $\dfrac{\partial\dot\tau_1(u,X)}{\partial u}=\dfrac{1}{c}\left[\dfrac{v^2-\dot r_1^2(u)}{r_1(u)}\right]$ and

$$\nabla_X\dot\tau_1(u,X)=\begin{pmatrix} \dfrac{\dot x}{c\, r_1(u)}-\dfrac{\dot r_1(u)}{c\, r_1^2(u)}(x-x_1+u\dot x) \\ \dfrac{\dot y}{c\, r_1(u)}-\dfrac{\dot r_1(u)}{c\ r_1^2(u)}(y-y_1+u\dot y) \\ \dfrac{\dot x-x_1+2u\dot x}{c\, r_1(u)}-u\,\dfrac{\dot r_1(u)}{c\, r_1^2(u)}(x-x_1+u\dot x) \\ \dfrac{\dot y-y_1+2u\dot y}{c\, r_1(u)}-u\,\dfrac{\dot r_1(u)}{c\, r_1^2(u)}(y-y_1+u\dot y)\end{pmatrix}$$

REFERENCES

[1] H. Cox, "Fundamentals of Bistatic Active Sonar", in Y.T. Chan (ed.), Underwater Data Processing, Kluwer Academic Publishers, 1989, pp. 3–24.

[2] P.T. Gough, A. De Roos, and M.J. Cusdin, "Continuous Transmission FM Sonar with One Octave Bandwidth and no Blind Time", IEE Proceedings, Part F, vol. 131, no. 3, pp. 270–274, Jun. 1984.

[3] H.A. DeFerrari, "The Application of m-Sequences to Bi-static Active Sonar", Journal of the Acoustical Society of America, vol. 114, p. 2399, 2003.

[4] H. DeFerrari, H. Nguyen, and A. Rogers, "Continuous active pulse compression sonar", Proceedings of the International Conference on Underwater Acoustic Measurements – Technologies & Results, Crete, 2005.

[5] T.C. Yang, "Acoustic Dopplergram for Intruder Defense", IEEE Ocean 2007, pp. 1–5.

[6] P. Blanc-Benon, D. Pilllon, and J. Clavard, "CAS TMA Applied for Sonobuoys in MPA Context", Underwater Defense and Technology Conference, UDT 2012, Alicante, Spain.

[7] B.H. Maranda, "The Statistical Accuracy of an Arctangent Bearing Estimator", in Proceedings of OCEANS 2003, vol. 4, San Diego, USA, 2003, pp. 2127–2132.

[8] C. Jauffret and A.C. Pignol, "Target Motion Analysis by Inverse Triangulation", 18th International Conference on Information Fusion, Washington, USA, Jul. 2015, pp. 507–514.

[9] C. Jauffret, "Observability and Fisher Information Matrix in Nonlinear Regression", IEEE Transactions on Aerospace and Electronic Systems, vol. 43, no. 2, pp. 756–759, Apr. 2007.

[10] J. Liang, L. Xu, J. Li, and P. Stoica, "On Designing the Transmission and Reception of Multistatic Continuous Active Sonar", IEEE Transactions on Aerospace and Electronic Systems, vol. 50, no. 1, pp. 285–299, Jan. 2014.

[11] Y.C. Xiao, P. Wei, and T. Yuan, "Observability and Performance Analysis of Bi/Multi-static Doppler-Only Radar", IEEE Transactions on Aerospace and Electronic Systems, vol. 46, no. 1654–1667, pp. 285–299, Oct. 2010.

[12] OCEANS'15, Continuous Active Sonar session, MTS/IEEE Proceedings, Genova, Italy, 2015.